INL-RPT-21-66504
Revision 0

Modeling of Radiolytic Hydrogen Generation of Irradiated Surrogate Aluminum Plates

March 2022

Alexander Abboud

Changing the World's Energy Future

Idaho National Laboratory

INL is a U.S. Department of Energy National Laboratory operated by Battelle Energy Alliance, LLC

INL-RPT-21-66504
Revision 0

Modeling of Radiolytic Hydrogen Generation of Irradiated Surrogate Aluminum Plates

Alexander Abboud

March 2022

Idaho National Laboratory
Idaho Falls, Idaho 83415

http://www.inl.gov

Prepared for the
U.S. Department of Energy
Office of Environmental Management
Under DOE Idaho Operations Office
Contract DE-AC07-05ID14517

Page intentionally left blank

SUMMARY

The hydrogen generation from oxyhydroxide layers under irradiation is an important effect to understand for the long-term storage of aluminum-clad spent nuclear fuel. The original chemical model shows steady production of hydrogen from aluminum oxyhydroxide layers, with no roll-over effect in the curves of the hydrogen concentration until significant pressure has built up within the canister. This study uses a variety of kinetic fits to adjust the old chemical model to have roll-over effects that are consistent with new high-dose experiments. The data from aluminum 6061 coupon tests at high doses were used to fit several kinetic models. The 6061 aluminum samples are representative of the aluminum-clad fuel from the ATR. The fitted kinetic models were then used in a model of a mini-canister with much higher packing density to determine which kinetic rates would fit both sets of experimental tests. The rate constants for the kinetic mechanisms that were close were then tweaked such that the chemical models fit both the experimental data from the capsule tests and the data from the mini-canister tests. The kinetic models which fit the best are either inhibition by hydrogen, or a back reaction wherein H radical is reabsorbed onto the oxyhydroxide layer. The H back reaction rolls over quicker and may fit future collected data.

ACKNOWLEDGEMENTS

This work was funded by the U.S. Department of Energy Environmental Management office. This work was performed by Battelle Energy Alliance, LLC, under DOE Idaho Operations Contract DE-AC07-05ID14517 and made use of the resources of the High Performance Computing Center at Idaho National Laboratory which is supported by the Office of Nuclear Energy of the U.S. DOE and the Nuclear Science User Facilities.

CONTENTS

FIGURES

Page intentionally left blank

ACRONYMS

ATR	Advanced Test Reactor
ASNF	Aluminum-clad Spent Nuclear Fuel
CFD	Computational Fluid Dynamics
DOE	Department of Energy
INL	Idaho National Laboratory
SRNL	Savannah River National Laboratory
SNF	Spent Nuclear Fuel

Page intentionally left blank

Modeling of Radiolytic Hydrogen Generation of Irradiated Surrogate Aluminum Plates

1. Introduction

By the year 2035, there will be ~2500 MTHM of spent nuclear fuel (SNF) that will require geologic repository disposal that is managed by DOE. Approximately 400 MHTM of this is currently not packaged (SNFWG, 2017). Previous studies in support of geologic disposal divided the DOE SNF inventory into 34 groups based on fuel matrix, cladding, cladding condition, and enrichment (SNFWG, 2017). The six aluminum clad fuel types are of interest as aluminum is significantly less corrosion resistant than stainless steel and zircaloy clad fuel. The aluminum cladding develops a corrosion layer that generates hydrogen from radiolysis, and that contain bound, both physiosorbed and chemisorbed, water.

Over 30% of the volume of DOE stored fuel is aluminum clad. One source of the aluminum spent nuclear fuel (ASNF) that will continue to be produced and needs to be stored is the advanced test reactor (ATR) fuel at the Idaho National Laboratory. The disposition path for this ASNF is to be loaded into road-ready DOE sealed canisters back filled with helium for transportation and long-term storage. A previous report examined the chemical contents within this DOE canisters using a set of radiolytic chemistry reactions for both the gas and the aluminum surface. The previous report utilized G-values for the surface reactions in an argon atmosphere, but recent experimental tests have shown that a helium environment has higher hydrogen generation rates (Parker-Quaife and Horne, 2021). These tests also show deviation from linearity with increasing dose, indicating a potential steady-state H_2 concentration, though higher dose samples are to be evaluated. Follow up tests have bene completed which show the roll-over effect at high doses but have not been published yet. This data is used to modify the previous chemical model to address this effect.

The model in this study is only a chemical model, but in the future will be coupled with the CFD model of the full-scale DOE sealed standard canister (Abboud Huang 2019; Abboud and Huang 2020; Abboud 2021). Past CFD models have not coupled the thermal and convective fields with the harmful chemical species which occur due to the radiolytic breakdown of water vapor, nitrogen, oxygen and carbon dioxide that is present within vented canisters (Wittman and Hanson 2015; Arkhipov 2007; Atkinson 2004). In addition, the past CFD models have not looked at the transient evolution of the thermal fields inside canisters, opting for steady state solutions. The transient solution allows for the model to track the concentration of hydrogen and other species over long time periods as the fuel's decay heat decreases.

This study solves the chemical state of the evolution of sealed mini-canister mockups placed in an irradiator at Savannah River National Laboratory (SRNL) (Verst and d'Entremont 2021). The previous model is first used to create a prediction on hydrogen generation with constant G-values. However, utilizing constant G-values over the time frame of the experiments results in an overprediction in hydrogen generation, as the experiments show an early roll-over occurring in hydrogen production. A variety of kinetic models are fit to high-dose experimental data from capsule tests that were performed by Idaho National Laboratory (INL). The kinetic rates fit to the capsules were then utilized in the model for the mini-canister to determine the best fit for the chemical models to use in the future.

2. Theory and Model Description

2.1 Thermal Fluid Model

Unlike the model of the full-sized canister, no CFD model is done here. The mini-canister is assumed to be at 25 C for the chemical model.

2.2 Gas-Phase Chemical Equations

The chemical reactions which are considered are one-step reactions. In the vented system, the full chemical reaction mechanism from Wittman & Hanson, 2015, was considered to begin with. This full mechanism contains 40 chemical species and 115 total reactions. This model was developed from literature for a full set of chemical reactions using prior experimental collection of radiolysis data (Bulearca et al., 2010, Atkinson et al., 2004; Arkhipov et al., 2007), and was used in the initial model of the DOE sealed standard canister without surface chemistry (Abboud 2022). Due to the nature of the time period interest of this study, it would be infeasible to fully resolve all 40 chemical species and 115 total reactions within the canister due to the computational cost of multiphysics CFD models.

The model utilizes Cantera for solution of the chemical reactions. Cantera software was used on the full set of reactions listed by Wittman & Hanson (2015) to determine other non-radical species that could be ignored in the analysis, several species such as HO_2, H_2O_2, NH_3, and many others would exist only at parts-per-trillions amounts even after a 50-year batch reactor model was completed, so these species were ignored in the helium-filled canisters. The source term of chemical species is

$$\frac{d[A_i]}{dt} = \dot{d}\sum G_i w_g[A_g] + \sum k_{ir}\prod[A_{jr}]^{O_{jr}} \tag{1}$$

Where $\dot{d}$ is the dose rate, G_i is the G-value for the radiolytic decomposition, w_g is the molecular weight, k_{ir} is the reaction rate, and O_{jr} is the reaction order for species j. The transport equations for the species mass fractions, Y_i, are solved for N-1 species as

$$\frac{\partial \rho Y_i}{\partial t} + \nabla \cdot (\rho v Y_i) = \nabla \cdot \left(J_i + \frac{\mu_t}{\sigma_t}\nabla Y_i\right) + S_{Y_i} \tag{2}$$

The source term here, S_{Y_i}, is reformulated from equation 7 to be in terms of the mass fractions rather than concentration. The basic diffusion is defined as

$$J_i = \rho D_{i,m} \nabla Y_i \tag{3}$$

Where $D_{i,m}$ is the binary diffusion coefficient. The general reaction term is defined as

$$k_{ir} = k_{ir}^0 T^{x_r} \exp\left(-\frac{E_a}{RT}\right) \tag{4}$$

2.3 Surface Chemistry

The prior modeling efforts describe the cover gas chemical phases, which are solved through Cantera. Based on the work completed by associated tasks in the ongoing investigations into storage of aluminum-clad spent nuclear fuel, the surface chemistry associated with the aluminum cladding was added into the model. This is done through work outlined for the radiolytic yield of the aluminum hydroxide (Zalupski 2018), the general surface corrosion (Lister 2018), and prior kinetic expressions for aluminum corrosion. The surface chemistry built in Cantera is intended for catalytic reactions, though it is utilized here, it allows for all parts of the metal to be reactive even if not at the surface. However, this estimate is a conservative approximation, so it should provide an upper bound. In creating the surface, first the number of moles of AlOOH present is calculated based on the plate thickness, and surface area of the plates

$$n_{AlOOH} = \frac{A_{fuel} th_{AlOOH} \rho_{AlOOH}}{MW_{AlOOH}} \tag{5}$$

And the ratio of moles of oxide to moles of aluminum alloy is assumed proportional to the film thickness and the plate thickness

$$\theta_{AlOOH} = \frac{th_{AlOOH}}{th_{plate}/2} \tag{6}$$

While this may underestimate total aluminum present to have a single surface, it is not that reactive at low temperatures. The calculation of the site density with this assumption is then

$$\rho_s = \frac{n_{AlOOH}}{X_{AlOOH} A_{fuel}} \tag{7}$$

The moles present for reaction is then

$$[\mathrm{AlOOH}] = \theta_{AlOOH}\rho_s \tag{8}$$

With this formulation of the surface sites, the following reaction is implemented for radiolysis of boehmite film

$$2\ \mathrm{AlOOH(S)} \xrightarrow{\gamma} 2\ \mathrm{AlOO(S)} + 2\ \mathrm{H}\cdot \tag{9}$$

With the hydrogen radical determined through a combination of model tuning, and atomistic theory (Westbrook et al. 2015). The G-value used here was updated from the previous work to be specific to a helium back-filled environment. For relative humidity of 100% the G-value is 4.12x 10^{-4} μmol/J, and for relative humidity of 50%, the G-value is 2.92 x 10^{-4} μmol/J, applied to the entire sample mass. This is a change from previous modeling efforts, which applied the G-value only to the mass of oxyhydroxide layer using the G-values from (Parker-Quaife and Horne, 2021). This effectively changes the reaction from 1st order with regards to the corrosion layer to 0th order. Another reaction is included with a slow rate to convert the intermediate AlOO to stable Al_2O_3. The thermal dehydration of boehmite at low temperatures was also considered. The mass loss of aluminum oxyhydroxide coupons was considered to be from the loss of water in determining the kinetic rate according to the reaction

$$\mathrm{AlOOH}\cdot(1.5\ \mathrm{H_2O})(\mathrm{S}) \leftrightarrow 2\ \mathrm{ALOOH(S)} + 1.5\ \mathrm{H_2O(g)} \tag{10}$$

This reaction was fit to the mass loss of the coupons ranging from 25 to 180 °C (Lister and Orme 2019). For a conservative approximation on undried cases, the upper end of pseudo boehmite was assumed with a 2.5:1 H_2O to Al_2O_3 ratio (Vedder and Vermilyea 1969). Lastly, the general corrosion of aluminum in the event that the oxyhydroxide layer was consumed was also considered from an older study (Hilton, 2000). This reaction was adapted from aluminum in water rather than humid air, and so should be conservative to include

$$\mathrm{Al(S)} + 1.5\ \mathrm{H_2O} \rightarrow 0.5\ \mathrm{Al_2O_3(S)} + 1.5\mathrm{H_2(g)} \tag{11}$$

Though it should be noted this last equation has a most minimal effect. At an average surface temperature of 50 °C, the total aluminum corrosion would only equation to 1.2 grams after 50 years, or 58 grams after 50 years at 200 °C surface temperature.

2.3.1 Roll-over effect of Surface Chemistry

A set of simple models were tested and fit to the capsule data experiments to get a rollover type effect. The reaction order was assumed to be only dependent on the gas phase. The kinetics rates tried were back reactions that reach an equilibrium, inhibition of the reaction rate based on hydrogen gas concentrations, or simply fitting an exponential decay curve to the G-value. An alternative of the back reactions shown could also be to combine the H atom with the proper ratio of Al_2O_3 on the surface with

Al as a product (i.e., [4/3 Al_2O_3 + H_2 → 2 AlOOH + 2/3 Al] instead of [2 AlOO + H_2 → 2 AlOOH]), but with the dependency fixed to the gas phase this characterization doesn't affect the rate here. This assumption can be revisited in the future if needed. The kinetic fits that were tried were

- 1st order back reaction H_2 (2 AlOO + H_2 → 2 AlOOH)
- 1/2 order back reaction H_2 (AlOO + 0.5 H_2 → AlOOH)
- 1st order back reaction H· (AlOO + H· → AlOOH)
- 2nd order back reaction H· (2 AlOO + 2H· → 2 AlOOH)
- Inhibition by H· (k_{ir} = A [H]/(1 + B H))
- Inhibition by H_2 (k_{ir} = A [H_2]/(1 + B [H_2]))
- Fitting G-value ~ A exp(-B [H_2])

2.4 Model Geometry

Since no fully couple CFD model is done to match the constant temperature experiments, the model geometry is only important in determining the parameters to feed into the Cantera chemical model. The information for the aluminum surrogate samples were used to determine the free volume, surface area, and aluminum mass to use. Figure 1a shows the vessel and Figure 1b shows the surrogate aluminum plates for the tests performed at SRNL. The dose rate was determined to be 49500 rad/hr or 0.1375 Gy/s (Verst and d'Entremont 2021).

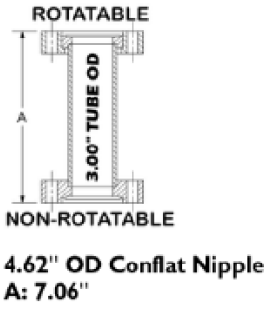

(a)

(b)

Figure 1. The (a) vessel container and the (b) surrogate aluminum plates.

For the model of the capsule, the surface area of the aluminum coupons was calculated to be 1.82 x 10^{-4} m^2. The approximate average for the coupon mass was used as 0.68 grams, and the free volume of the capsule was assumed to be about 1.0 x 10^{-5} m^3. For the large plate model, the fuel mass was taken as the measured value of 616.7 grams. The dimensions of the aluminum plates and the hardware were used to determine the surface area of the entire setup as 0.399 m^2. The calculated volume of the aluminum plates was subtracted from the total volume of the interior of the cylindrical device and determined to be 4.98 x 10^{-4} m^3. This results in a 182-fold increase in mass/free volume ratio and a 44-fold increase in surface area/free volume ratio from the capsule to the large plate experiments, which produces the roll-over effect at lower total doses in the experiments and should have the same effect in the chemical model. In addition, the mini canister has a decrease in the pressure as samples are withdrawn from the vessel. This is done at fixed intervals within the model based on the average of the reported sampling times of the experiments at 1.1 x 10^6 s. Both models are assumed to have an initial cover gas of pure helium.

3. Results and Discussion

3.1 Capsule Model

The model was run for the kinetic fits discussed in Section 2.3.1. The total time was run such that 1.0 x 10^8 Gy of total dose were achieved. The rate constants for each of the kinetic mechanisms was fit to show agreement with the experimental data. Figure 2a shows the results of the chemical model for the full-time frame. The thin blue line shows the model results with a constant G-value from the previous model. The result of the differing kinetic models to achieve a roll-over effect show significantly lower hydrogen generation rates than the constant G-value model. Figure 2b shows the same data but is truncated near the limits of the experimental data. The experimental data is shown with the red circles and the associated error bars. The units are the same H_2 µmol/kg reported from the capsule experiments.

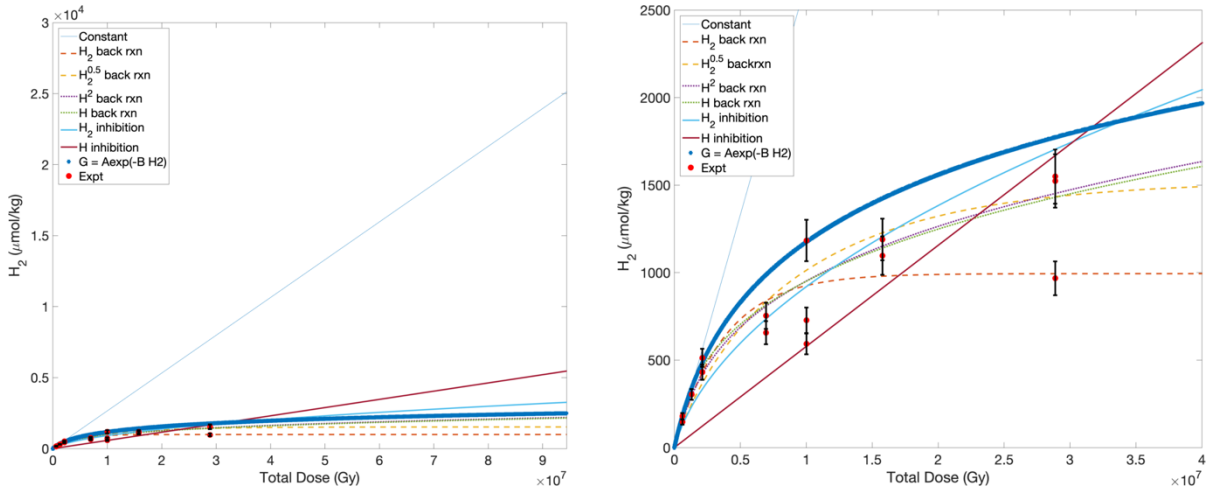

(a) (b)

Figure 2. The initial chemical model results for the capsule (a) full time frame and the (b) short term time frame corresponding to experimental data.

The fit for the exponential decay over predicts data towards the end as its fit is based on tabulated G-value data by the individual points. But this does provide a fit that bounds the experimental data set. The inhibition reaction by H radical has a problem with fitting the roll-over effect at low dose rates and gives the highest prediction at long times. The H_2 inhibition shows some error in the roll-over area, but is much better than the H inhibition, a low dose under 5 million Gy and has the second highest prediction at longer time frames. A back reaction rate based on the H radical shows nearly the same result for both the fit on the first-order and second-order back reaction, and both have a continued slow production rate beyond the experimental time frame, but these model both capture the initial roll-over effect at low doses. The two models based on the H_2 back reaction of one-half-order and first-order also capture the initial roll over effect, but show an equilibrium reached much faster than the back reactions of the H radical. The spread on these different models is over 1000 µmol/kg at short time frames. To achieve a model that would work for a variety of systems the models are also run with the same kinetic rates in the mini-canister system.

3.2 Mini-Canister Model

The initial model for the mini-canister used the same kinetic rate constants that were fit to the capsule experimental data shown in Figure 2. As with the capsule model, the mini-canister model was run for a longer period of time than that of the experimental data to provide longer-term predictions that could be used in the full-scale model later, and also if additional data becomes available. The model data for the mini canister is plotted as the time versus the hydrogen mole fraction. The model for the full timeframe is

shown in Figure 3a, and a truncated set of model data around the experimental limits is shown in Figure 3b. The experimental data is shown in red circles, no error is reported for the mini-canister tests, but was assumed to be the same percentage as the capsule data.

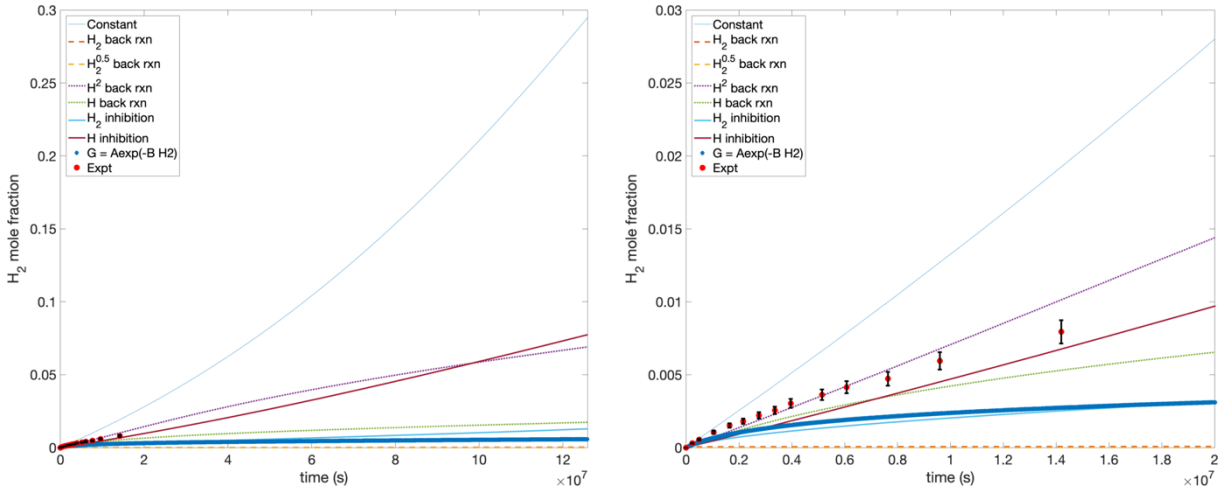

Figure 3. The initial chemical model results for the mini-canister (a) full time frame and the (b) short term time frame corresponding to experimental data.

The kinetic fits to the mini-canister model show a much higher spread than that of the capsule model data due to the large difference in the ratio of material to free volume between the cases. At high time frames the constant G-value concentration ramps up as the continued pressure drop form withdrawal occurs. The fit to the exponential decay for the G-value underpredicts the production greatly, as the concentrations in the mini-canister reach a higher concentration much quicker than the capsule tests. The two models for the back reaction via H_2 for both the one-half-order and first-order show negligible amounts of hydrogen generated for the mini-canister model. The back reaction for the H radical for both the second-order and first-order reaction straddle the experimental data set with the previously fit rate constants. The inhibition reaction of H is nearly linear for this period, as it was in the capsule data set. The inhibition reaction of H_2 underpredicts the long-term data but shows some agreement with the short-time frame data.

As the capsule experimental data has a large spread in the high-dose experimental data, the model runs that were shown in Figure 2 could have rate constants adjusted and while not optimized to minimize error as before, could have model data that still lies within the bounds of the experimental error. In order to adjust the models, the kinetic rate constants from the capsule data were refitted to the mini canister data set. The G-value in the forward reaction was increased slightly so that the earlier portion of the slope is captured better, and this allows for faster backward reaction rates to be used to capture the roll-over effect better. The focus of the refitting of the kinetic rates was limited to the mechanisms with the potential to match the data well with small changes, these were the first-order and second-order back reactions with H radical, and the H_2 inhibition. The refitted models for the mini-canister are shown in Figure 4a for the full time frame and in Figure 4b for the truncated time frame.

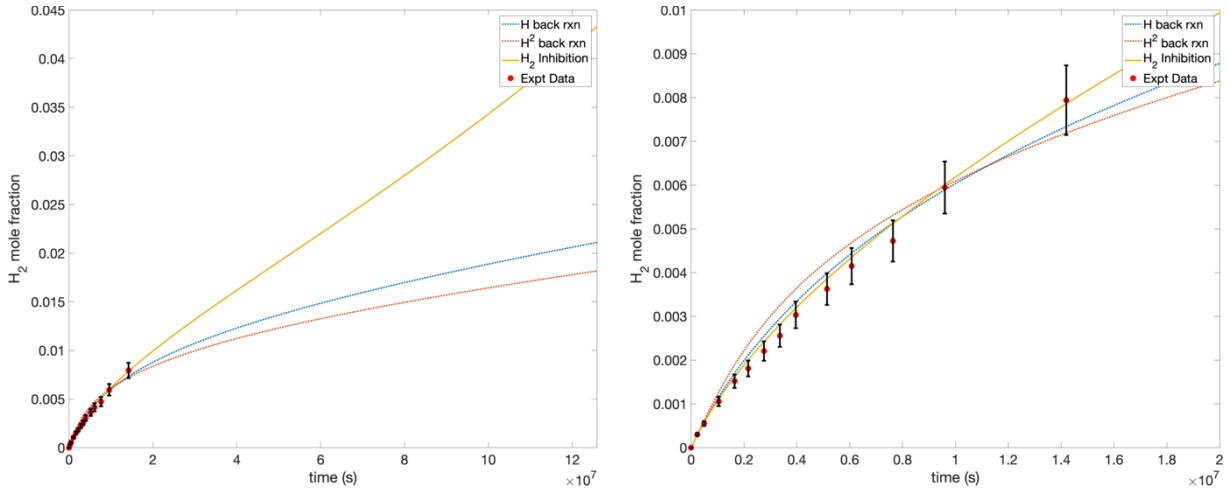

(a) (b)

Figure 4. The chemical model results for the re-fit model of the mini-canister (a) full time frame and the (b) short term time frame corresponding to experimental data.

All three of the fits shown match the experimental canister data well during the timeframe for which data is available. The H_2 inhibition shows significant increases in the concentration at longer time periods. Part of this is due to the continued withdrawal of air from the mini-canister model. As air is withdrawn, the pressure drops, decreasing the hydrogen concentrations and therefore increasing the forward rate constant. The mini-canister system was run again for these new rates, but after the experimental data timeframe has ended, the withdrawal amount has been decreased by a factor of five. The hydrogen data for this updated mini-canister model is shown in Figure 5a, and the pressure data in comparison with the initial model is shown in Figure 5b. This model shows nearly a 50% reduction in hydrogen for the inhibition case, and the pressure with this slower withdrawal maintains about an atmosphere by the end of the modeled timeframe.

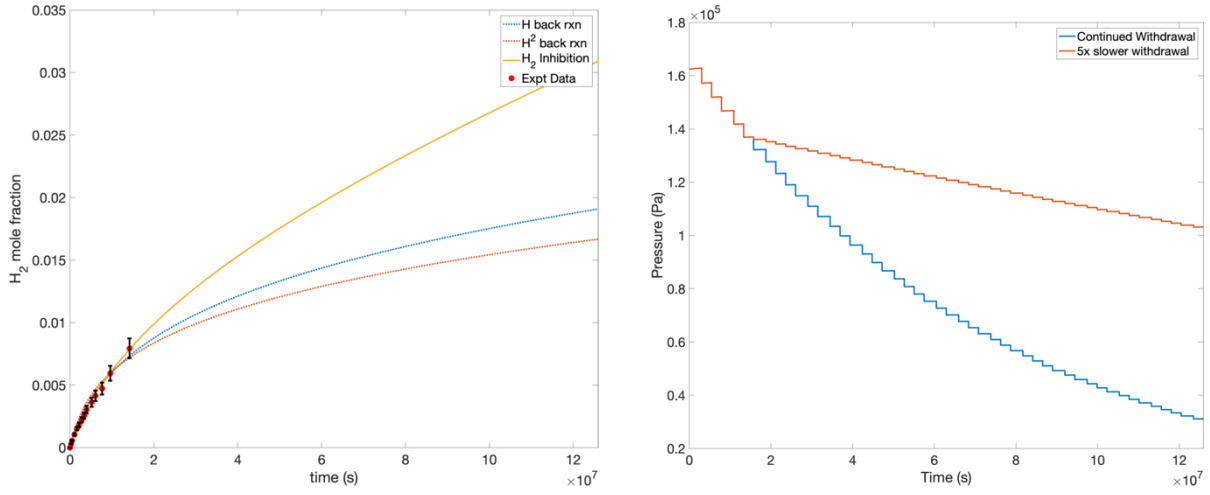

(a) (b)

Figure 5. The chemical model results for the re-fit model of the mini-canister with slow withdrawal (a) full time frame and the (b) pressure compared to original model.

3.3 Final Model Fit

The rate constants from the updated kinetic models shown in Figure 5 were then used in the capsule model. The updated capsule model data is shown in Figure 6a for the full timeframe and for Figure 6b for the truncated time frame near the experimental data. This updated model shows that the back reaction from H radical as a second-order reaction shows data far lower than the experimental data. The hydrogen inhibition reaction and H radical first-order back reaction are then the mechanisms modeled which fit both the capsule experimental data and the mini-canister experimental data well. Since the H radical back reaction has not quite completed its full roll-over, this model could be used as a conservative estimate for the full model in the DOE standard sealed canister, and the H_2 inhibition rate can be used for the lower bounds of the model.

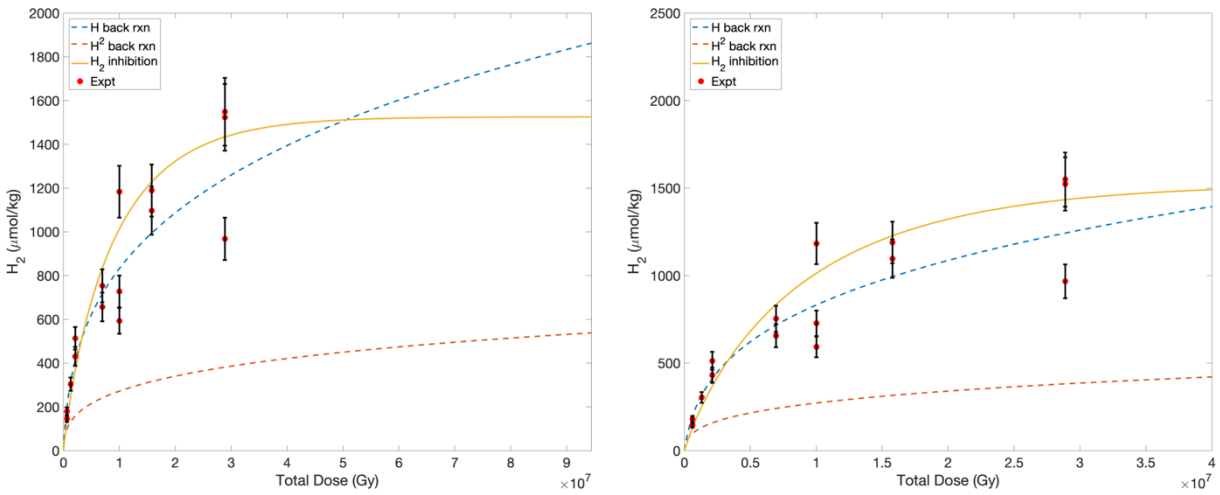

Figure 6. The chemical model results for the re-fit model of the capsule for (a) full time frame and the (b) short term time frame corresponding to experimental data.

The two models to be considered for future modeling for the full timeframe are shown in Figure 7a for the capsule model and in Figure 7b for the mini-canister model. The minor species of the capsule model on a log scale are shown in Figure 7c. In the updated chemical model, as with the original model, no other species except hydrogen is present in any large quantity. The minor species of the mini-canister model are shown in Figure 7d, with its much higher hydrogen concentration. As with the capsule model, no other species are significant in large quantities. For the models suggest there may be additional hydrogen generation within the capsules and mini-canister as total dose is increased, albeit at a much lower generation rate.

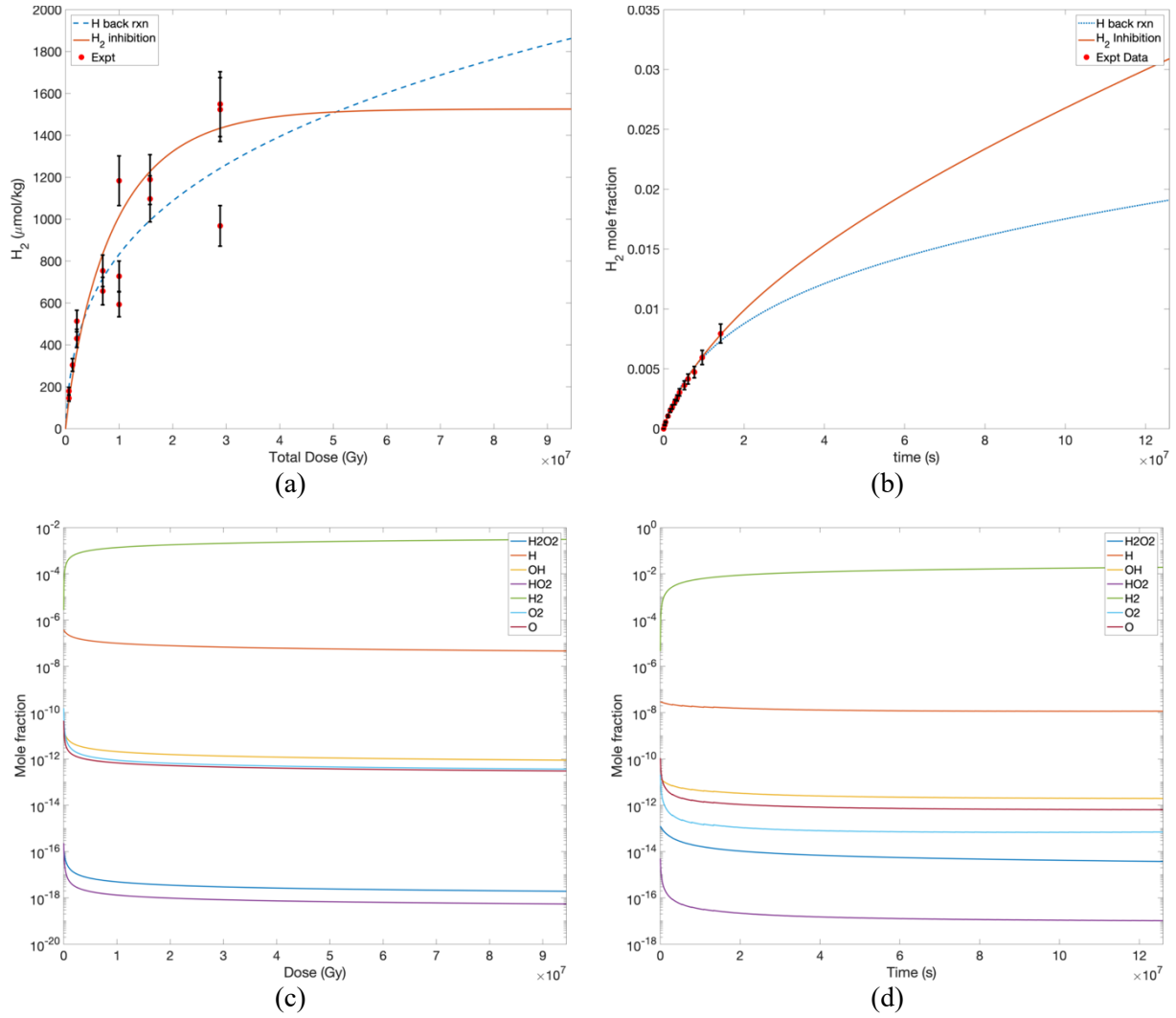

Figure 7. The final model results for the (a) capsule model and (b) mini-canister model. The minor species for the H radical back reaction for the (c) capsule model and (d) mini-canister model.

The SRNL dataset also included a set of aluminum 6061T6 plates that were dried before being irradiated. This set of data did not have a completed one-to-one test for the capsule experiments at INL. For a first cut of the model, the same rate constants used for the H back reaction was used, but the G-value for the forward reaction was decreased to 9.35 x 10^{-5} to match the initial spike in the measured G-value from the experiments. The H_2 inhibition reaction was also tested with the same rate constant, however, this test failed to match the experimental data well, so a second fit for this mechanism was created for the dried plate mini-canister test. The comparison of the model fit for the dried test is shown in Figure 8a for the long-term time frame and in Figure 8b for the short-term time frame. The model shows that the equilibrium has not been achieved yet and low generation of hydrogen may continue. The model can be updated if additional experimental data becomes available.

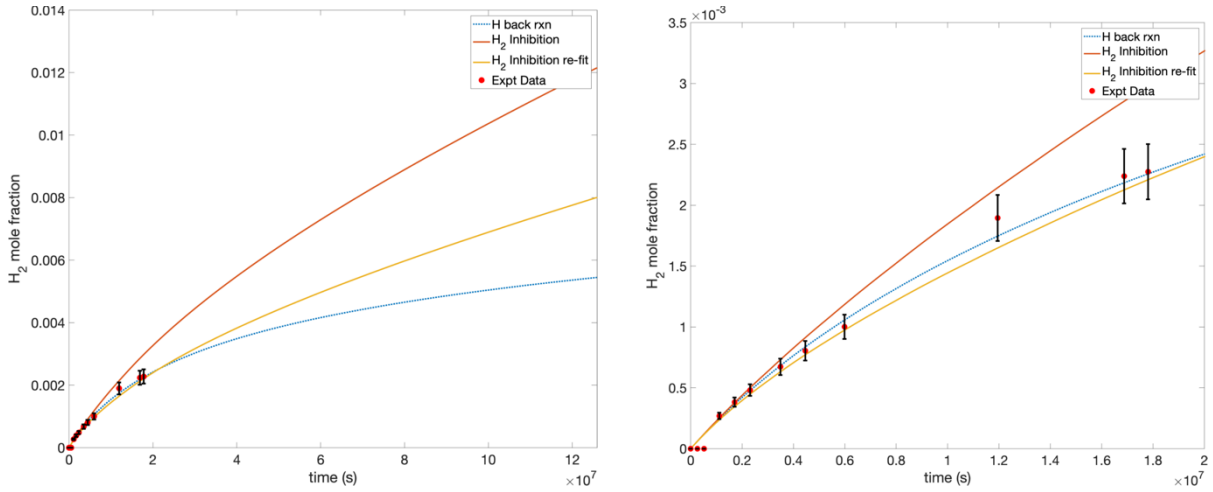

(a) (b)

Figure 8. The model results for the dried plate mini-canister model for (a) the full timeframe and (b) short term time frame corresponding to experimental data.

4. Conclusions

The experiment data for high-dose capsule experiments was used to fit kinetic parameters to adapt the chemical model for the roll-over effect seen within high-dose experiments. The fitted rate constants were then used to create a model of the mini-canister experimental test with a high packing density. The model seems to point to either the back reaction of H radical reabsorbing on the surface to form chemical equilibrium, or inhibition of the reaction based on the hydrogen concentration in the gas phase. If additional experimental data becomes available, the kinetic rate constants can be refitted to adapt to the new data.

The next steps are to update the model of the full-sized DOE standard sealed canister with this new kinetic rate constant data so that it more accurately represents the roll-over effect seen experimentally at high doses. This DOE standard sealed canister model will be expanded out to a longer-term such that roll-over and/or final equilibrium of the model is achieved. A model will also be constructed of the one-third scale DOE sealed canister and the hydrogen content will be calculated to provide validation test of the coupled CFD-chemical model for the full-sized canister system.

REFERENCES

Abboud A.W. and Huang, H., 2018. Transient Coupled Chemical-Thermal-Fluid Field Simulation of Sealed Aluminum-clad Spent Nuclear Fuel Storage Canister, Tech. rep. INL/EXT-18-51683.

Abboud A.W. and Huang, H., 2019. Sensitivity Study of Coupled Chemical-CFD Simulations for Sealed and Unsealed Aluminum-clad Spent Nuclear Fuel Storage Canisters. Idaho National Laboratory, Tech. rep. INL/EXT-19-52650.

Abboud A.W., 2021. Modeling Summary of ASNF in DOE Sealed Standard Canisters, Tech. rep. INL/EXT-21-64413.

Abboud, A. W. (2022). Sensitivity study of coupled chemical-CFD simulations for analyzing aluminum-clad spent nuclear fuel storage in sealed canisters. Nuclear Engineering and Design, 390, 111691.

Arkhipov, O.P., Verkhovskaya, A.O., Kabakchi, S.A., and Ermakov, A.N., 2007. Development and verification of a mathematical model of the radiolysis of water vapor. Atomic Energy, 103(5):870.

Atkinson, R., Baulch, D.L., Cox, R.A., Crowley, J.N., Hampson, R.F., Hynes, R.G., Jenkin, M.E., Rossie, M.J., and Troe, J., 2004. Evaluated kinetic and photochemical data for atmospheric chemistry: volume I – gas phase reactions of X, HOx, NO2, and SOx species. Atmospheric Chemistry and Physics, 4(6): 1461-1738.

Bulearca, A.M., Calinescu, I., and Lavric, V., 2010. Model Studies of NOx and SOx reactions in Flue gas treatment by electron beam. UPB Sci Bull, Series B, 72(1):101-112.

Goodwin, D.G., Moffat, H.K., and Speth, R.L. *Cantera: An object-oriented software toolkit for chemical kinetics, thermodynamics, and transport processes*. http://www.cantera.org, 2017. Version 2.3.0. doi:10.5281/zenodo.170284

Olson, L., Verst, C., d'Entremont, A., Fuentes, R., Sindelar, R., 2019. Characterization of Oxide Films on Aluminum Materials following Reactor Exposure and Wet Storage in the SRS L-Basin. Tech. Rep. Savannah River National Laboratory, SRNL-STI-2019-00058.

Parker-Quaife E.H., Horne, G.P., Heathman, C.R., Verst, C., Zalupski, P.R. 2019. Radiation-Induced Molecular Hydrogen Gas Generation by Pre-Corroded Aluminum Alloy 1100. Tech Rep. Idaho National Laboratory, INL/EXT-19-55202.

Parker-Quaife E.H., Horne, G.P., 2021. Milestone 2.8: Preliminary Radiolytic Gas Generation Measurements from Helium-Backfilled Samples. Tech. Rep. Idaho National Laboratory, INL/EXT-21-61404.

Vedder, W. and Vermilyea, D.A. 1968. Aluminum + Water Reaction. Trans. Faraday Soc, 65, pp.5 61-584.

Verst, C.G. and d'Entremont A.L. Measurement of Radiolytic Hydrogen Generation and Impact of Drying Treatments on Reactor-Exposed and Surrogate Aluminum Materials. Tech. rep. Savannah River National Laboratory, November 2021. SRNL-STI-2021-625.

Wittman, R., Hanson, B., 2015. Radiolysis model analysis for a used fuel storage canister. In proceedings: IHLRWM April 2015.

Westbrook, M.L., Sindelar, R.L., Fisher, D.L. 2015. Radiolytic hydrogen generation from aluminum oxyhydroxide solids: theory and experiment. J. Radioanal. Nucl. Chem., 303, pp 81-86.

Zalupski, P. 2018 Aluminum Clad Spent Nuclear Fuel Task 2: Oxide Layer Radiolytic Gas Generation Resolution Experiment Test Plan. Idaho National Laboratory, INL/EXT-18-45858.